

Probing Nanoscale Objects in Liquids through Membranes with Near-Field Microwave Microscopy

Alexander Tselev

Center for Nanophase Materials Sciences
Oak Ridge National Laboratory
Oak Ridge, TN 37831, USA
E-mail: atselev@utk.edu

Andrei Kolmakov

Center for Nanoscale Science and Technology
National Institute of Standards and Technology
Gaithersburg, MD 20899, USA
E-mail: andrei.kolmakov@nist.gov

Abstract—In this work, scanning near-field microwave imaging was implemented to test the feasibility of the approach for in-situ studies of nanoscale objects immersed in liquids under thin dielectric membranes. It was found that mechanical strength and stability of SiN membranes on Si frames are sufficient for contact mode imaging in a standard AFM setup. Model polystyrene particles immersed in glycerol in contact with the membrane from the cavity side could be reliably detected. The probing depth of this imaging mode can be estimated to be approximately 100 nm.

Keywords—microwave imaging; scanning probe microscopy; impedance measurement; atomic force microscopy

I. INTRODUCTION

The fast development of nanotechnology enables study and control of materials and devices at the level down to single atoms. Valuable knowledge can be gained through observations of nanometer- and atomic-scale objects and events in operando such as living cells, photo- and electrochemical reactions. This need boosted the development of in-situ electron microscopy techniques with

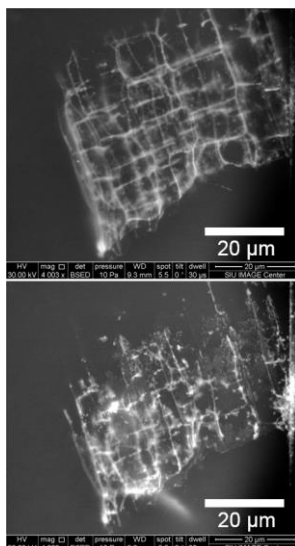


Fig. 1. Plant tissue immersed in water and imaged in an SEM through polyimide membrane. Top: Initial state; the image was acquired immediately after microscope adjustments at a neighboring spot. Bottom: the state after ca. 1 min. of exposure to the electron beam. The beam-induced degradation of the cellular walls is presumably due to water radiolysis and formation of chemically active species such as H_2O_2 .

samples imaged in liquid cells. In such cells, objects of interest are immersed in liquids confined by capsule-like structures, where one of the capsule dimensions is small enough to be transparent to electron beams [1]. However, electron energies and intensities in these experiments need to be high enough to penetrate through such membranes with acceptable attenuation. Typically, energies are in the tens of keV range for scanning electron microscopes (SEM) and hundreds of keV for transmission electron microscopes (TEM). Such energies are far above the thresholds for breaking chemical bonds in materials, which may eventually lead to sample destruction because of radiation-induced damage and unwanted chemical reactions. For example, 79 different chemical reactions were identified as occurring concurrently under an electron beam of a TEM in water [2]. The images in Fig. 1 show, for instance, a consequence of one-minute-long exposure of a plant tissue in water to electron beam of a 30 keV energy in an SEM. Apparent degradation of the cellular walls indicates that the radiation damage is unacceptably large for the selected imaging parameters. Similarly, electron damage and electron beam induced artifacts can be observed in many other soft matter objects such as polymers and electrolytes. Therefore, alternative imaging technique operating at smaller radiation energies are needed for radiation-sensitive specimens. Imaging using optical wavelengths would be an obvious candidate. However, the far-field optical imaging is limited in spatial resolution by diffraction effects. To achieve special resolution close to 100 nm and below, typical for in-situ electron microscopy of encapsulated samples, near-field imaging should be implemented. In a near-field, the special resolution limit is set by the scanning probe size rather than by the radiation wavelength, and one can use a radiation with wavelengths several orders of magnitude larger than the size of the probe or the field-concentrating element.

Microwave frequencies of about 1 GHz are the lowest where high-resolution near-field imaging was achieved [3]. Its important distinction is a very low energy photons - in the μeV range. At this energy scale, the energy is largely adsorbed by collective excitations in matter, and only heating can potentially lead to irreversible changes in the materials. Therefore, the radiolysis as well as radiation damage associated with the electron microscopies can be completely eliminated. Simultaneously, microwave radiation can penetrate into solids and liquids including those, which are opaque for optical radiation. As an example, microwaves were proposed for medical tomography and disease diagnostics [4-6] and used for underground and through-the-wall surveillance. In light of these properties, microwaves may have a significant potential for in-situ imaging objects in their native environment including biological, reactive, toxic, and others. While the history of near-field imaging goes back a few decades [3], the recent realization of the near-field microwave imaging on atomic-force microscopy (AFM) platforms with precise probe-sample distance control not only dramatically improves the spatial resolution [7-11], but also potentially offers new imaging capabilities taking advantage of penetrating ability of microwave fields [7, 9, 12, 13]

II. METHODS

The goal of this work was to analyze and experimentally prove the applicability of near-field microwave imaging for studies of objects immersed into liquids under a few tens nm thick dielectric membranes. The dielectric membranes serve as molecularly impermeable “walls” separating the liquids from the environment, however allowing the fields from the probe to reach the objects in the liquid. The main questions to be answered were the mechanical stability of the membrane under the AFM tip and the evaluation of the microscope sensitivity needed for informative imaging in this configuration.

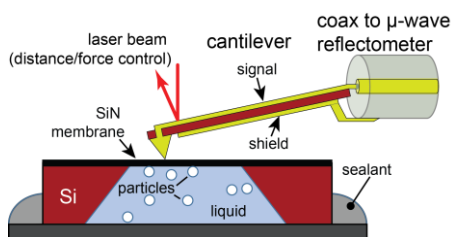


Fig. 2. Schematic of the experimental setup.

A. Experimental Setup

Fig. 2 displays a schematic of the near-field microwave imaging system employed in the experiments (Scan Wave, Prime Nano, Inc., Palo Alto, CA, USA). The probe is made as a standard AFM cantilever-based probe with a metallic sensing tip at the free cantilever end. The probe is completely shielded on the sample side, including the cantilever. The waveguiding structure runs to the very pyramid (sensing tip) and is geometrically close to a microstrip line. Importantly, the cantilevers are relatively soft with a spring constant of about 0.8 N/m, which can be used as advantage for imaging over thin membranes. The relatively moderate stiffness of the cantilevers allows for the formation of a mechanically and electrically stable contacts between the probe and the sample without the membrane being punched or moved by the probe while scanning, which is a necessary prerequisite for a successful AFM-based imaging.

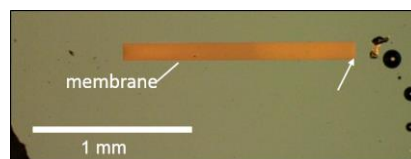


Fig. 3. Optical image of a membrane chip. The arrow indicated the corner, where images in Fig. 5 were acquired.

The probe is installed in a commercial AFM microscope with imaging performed with a probe in contact with the sample (contact mode). Generally, several images are obtained simultaneously within one scan frame corresponding to different microscope signals: height, deflection error, and microwave imaging channels.

The microwave detection system is based on the reflectometer principle. The amplitude and phase of the reflected waves are determined by the impedance of the tip-sample system, which is in turn determined by the average-over-cycle electric or magnetic energy stored in the near, evanescent, fields at the probe. For the tip-style probes, the energy is overwhelmingly stored in the electric component of the near fields, and therefore, the probes of this type are sensitive to sample dielectric permittivity and conductivity [3]. Accordingly, the output signals are provided as two channels: capacitive (C) and resistive (R), and this technique is named scanning Microwave Impedance Microscopy (sMIM). The probed sample volume is determined by the spatial extent and distribution of the fields. Since the electric field distribution has a singular character near the tip apex, the characteristic length scales in all three dimensions contributing to formation to the microscope signal and image contrast are defined by the tip apex radius. The nominal radius of the used tips is about 40 nm according to the manufacturer.

In the experiments, we used commercially available SiN membranes on Si frames designed as a support in TEM applications. We have chosen membranes of 50 nm thickness with the window shape shown in the optical image in Fig. 3. Such membranes are a good initial compromise between the membrane thickness and the mechanical strength. For the measurements, the cavities under the membranes were filled with glycerol. The high viscosity of glycerol was expected to facilitate the mechanical stability of the membrane under the localized pressure imposed by the probe. Prior to that, polystyrene particles of a diameter of $\approx 1.5 \mu\text{m}$ were placed in the cavity. The cavity was covered by a 10 mm-diameter steel disk and hermetically sealed with a glue. After that, the sMIM imaging was performed through the membrane at a microwave frequency of $\approx 3 \text{ GHz}$ and a generator power set to -20 dBm.

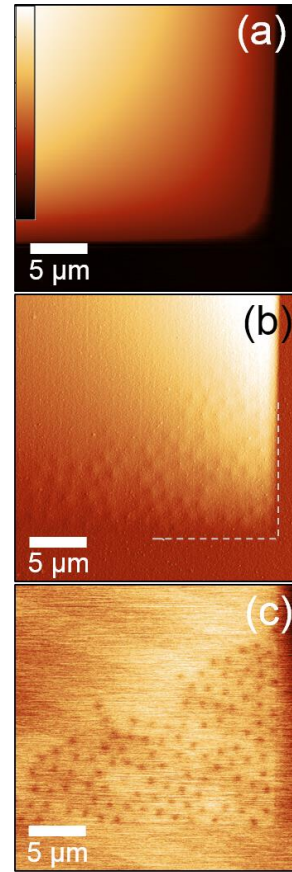


Fig. 5. (a) Height, (b) deflection error, and (c) sMIM-C images of a membrane window corner with agglomerated polystyrene particles in glycerol. The dashed line in (b) indicated the edge of the silicon substrate. See Fig. 3 as well. The full range of the color bar in (a) is 1.3 μm .

B. Numerical Modeling

To make an assessment of the applicability of the near-field microwave imaging for nanoscale objects immersed in liquids under a membrane, we have performed numerical calculations of the quasi-static electric field distribution in the tip-sample system in the presence of a particle in a glycerol. The modeling and calculations were carried out in quasi-static approximation employing a commercial finite elements analysis package. The model layout is displayed in Fig. 4. The model is axisymmetric. The tip is in contact with a membrane of a 50 nm thickness and a dielectric permittivity $\epsilon = 7.5$ (Si_3N_4). The space under the membrane is filled with a dielectric of a permittivity $\epsilon = 40$ (glycerol). A dielectric particle ($\epsilon = 2.5$) of a spherical shape and a diameter of 500 nm is in contact with the membrane from the cavity side. The tip-sample contact radius is set to 45 nm.

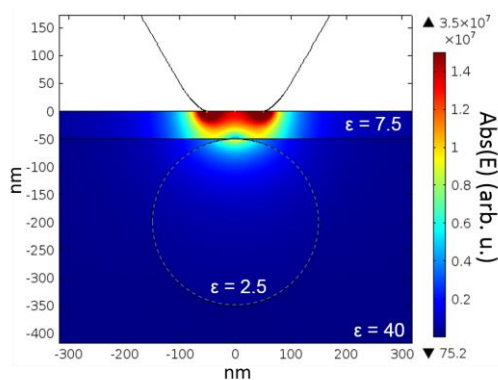


Fig. 4. Calculated distribution of the absolute value of the electric field near the probe tip apex in the presence of a dielectric particle.

III. RESULTS AND DISCUSSION

Fig. 4 show a calculated distribution of the electric field in the vicinity of the tip apex. As evident, there exists an appreciable coupling between the tip and the particle, however, only the top part of the particle can be accessed by the penetrating probing field. The calculation results also reveal a significant dielectric screening by the membrane due to a relatively large difference in the dielectric permittivities of SiN and glycerol.

Next, we performed imaging experiments with the setup described in the previous section. Fig. 5 presents one of typical sets of simultaneously acquired $25 \times 25 \mu\text{m}^2$ images of polystyrene particles in glycerol. The figure displays (from top to bottom) images of height, deflection error, and sMIM-C channel. In this particular case, the particles agglomerated in a corner of the membrane window. The particles are well visible against the background of glycerol. Both the particles ($\epsilon = 2.5$) and Si frame ($\epsilon = 12$) are darker in the image compared to glycerol ($\epsilon = 40$), as expected due to a higher dielectric constant of glycerol for the used microscope settings. The images also reveal a high stability of the membrane under scanning in contact mode. However, a significant fraction of the particles seen in the sMIM-C image appeared in the deflection error image as well, indicating the deformation of the membrane under the probe. This also evidences that the particles seen in the microwave image are in contact with the back side of the membrane. The structure formed by the particles is ordered with the main pattern corresponding to a hexagonal close-packed structure signaling that the particles are in contact with each other. Therefore, the distance between the particles in the images is equal to particles diameter. The image analysis reveals that the distances are narrowly distributed at the expected $1.5 \mu\text{m}$ corresponding to the nominal particle diameter. Since the apparent diameter of the darker spots in the sMIM-C image is about 0.25 to 0.4 of the particle diameter, the probed depth below the membrane can be preliminary estimated to be in the range from about 50 nm to 110 nm based on the spherical shape of the particles.

To further estimate the sensitivity and the spatial resolution of the microwave probing, we have imaged a smaller, $7 \times 7 \mu\text{m}^2$, region farther away from the membrane widow corner. For these images, the tip-sample set force was reduced by a factor of about 2.5. The height and sMIM-C images of an area with two isolated polystyrene particles under the membrane are shown in Figs. 6a and b. As seen, any signs of the particle presence are completely absent in the topographic image Fig. 6a; however, the image is streaky indicating some degree of instability in the tip-membrane contact causing the noise in the height image at a level of a few nm. Still, good-quality microwave images could be obtained. In the microwave image, the particle contrast has a characteristic profile expected for the spherical shape. The line profile across one of the spots in Fig. 6b shows a peak-like shape with base-line peak width of about $1.5 \mu\text{m}$ (Fig. 6c), suggesting that the signal variation is imposed by the whole particle diameter. It could be inferred that, in the tested configuration the sensitivity of the microwave imaging is sufficient for probing up to a depth of about $1 \mu\text{m}$ and even more. However, the influence of the probe side field has to be carefully analyzed and taken into account to verify this conclusion. Further experiments are planned to test the imaging mode in different liquid-particle configurations together with the numerical modeling and varying the membrane thicknesses.

IV. CONCLUSIONS

In conclusion, we have demonstrated the feasibility of the near-field microwave imaging for in-situ probing of nanoscale objects under thin membranes. The 50 nm thick SiN membrane stability and mechanical strength are adequate to enable contact mode imaging in a standard AFM setup with the membrane cavity filled with a viscous liquid. The sensitivity of the near-filed images used in the

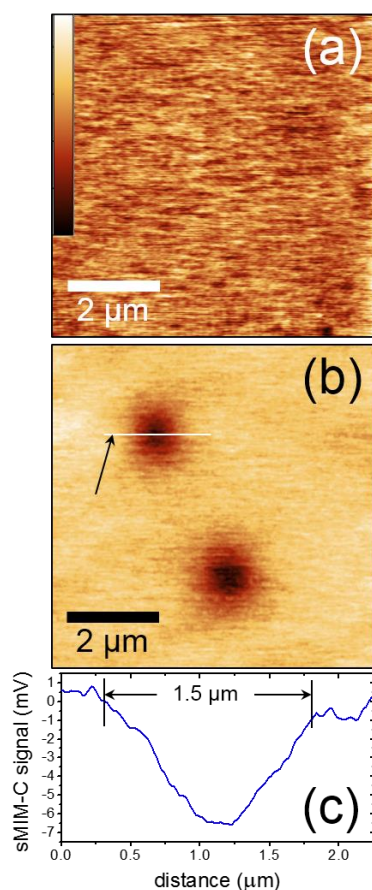


Fig. 6. (a) Height and (b) sMIM-C images of two isolated polystyrene particles under the membrane. (c) The sMIM-C signal profile along the line indicated by the arrow in (b). The full range of the color bar in (a) is 9.5 nm.

experiments was sufficient to detect polystyrene particles in glycerol in contact with the membrane. The probing depth can be estimated to be above 100 nm. Acknowledgment

Microwave imaging was conducted at the Center for Nanophase Materials Sciences, which also provided support (A. T.) and which is sponsored at Oak Ridge National Laboratory by the Scientific User Facilities Division, Office of Basic Energy Sciences, U. S. Department of Energy. A.T. acknowledges support by U.S. Civilian Research and Development Foundation.

Disclaimer: Certain commercial equipment, instruments, or materials are identified in this paper in order to demonstrate the experimental procedures and capabilities adequately. Such identification is not intended to imply recommendation or endorsement by the National Institute of Standards and Technology, nor is it intended to imply that the materials or equipment identified are necessarily the best available for the purpose.

REFERENCES

- [1] N. de Jonge and F. M. Ross, "Electron microscopy of specimens in liquid," *Nat. Nano*, vol. 6, pp. 695-704, 2011.
- [2] N. M. Schneider, M. M. Norton, B. J. Mendel, J. M. Grogan, F. M. Ross, and H. H. Bau, "Electron-Water Interactions and Implications for Liquid Cell Electron Microscopy," *J. Phys. Chem. C*, vol. 118, pp. 22373-22382, 2014.
- [3] S. M. Anlage, V. V. Talanov, and A. R. Schwartz, "Principles of Near-Field Microwave Microscopy," in *Scanning Probe Microscopy: Electrical and Electromechanical Phenomena at the Nanoscale*, S. Kalinin and A. Gruverman, Eds., ed New York: Springer Scientific, 2007, pp. 215-253.
- [4] S. Semenov, "Microwave tomography: review of the progress towards clinical applications," *Philosophical transactions. Series A, Mathematical, physical, and engineering sciences*, vol. 367, pp. 3021-3042, 2009.
- [5] K. P. Gaikovich, "Subsurface Near-Field Scanning Tomography," *Phys. Rev. Lett.*, vol. 98, p. 183902, 2007.
- [6] A. N. Reznik and N. V. Yurasova, "Electrodynamics of microwave Near-field probing: Application to medical diagnostics," *J. Appl. Phys.*, vol. 98, pp. 114701-9, 2005.
- [7] K. Lai, M. B. Ji, N. Leindecker, M. A. Kelly, and Z. X. Shen, "Atomic-force-microscope-compatible near-field scanning microwave microscope with separated excitation and sensing probes," *Rev. Sci. Instrum.*, vol. 78, p. 063702, 2007.

- [8] F. Wang, N. Clément, D. Ducatteau, D. Trodec, H. Tanbakuchi, B. Legrand, et al., "Quantitative impedance characterization of sub-10 nm scale capacitors and tunnel junctions with an interferometric scanning microwave microscope," *Nanotechnology*, vol. 25, p. 405703, 2014.
- [9] C. Plassard, E. Bourillot, J. Rossignol, Y. Lacroute, E. Lepleux, L. Pacheco, et al., "Detection of defects buried in metallic samples by scanning microwave microscopy," *Phys. Rev. B*, vol. 83, p. 121409, 2011.
- [10] S. Wu and J.-J. Yu, "Attofarad capacitance measurement corresponding to single-molecular level structural variations of self-assembled monolayers using scanning microwave microscopy," *Appl. Phys. Lett.*, vol. 97, p. 202902, 2010.
- [11] A. Tselev, N. V. Lavrik, I. Vlasiouk, D. P. Briggs, M. Rutgers, R. Proksch, et al., "Near-field microwave scanning probe imaging of conductivity inhomogeneities in CVD graphene," *Nanotechnology*, vol. 23, p. 385706, 2012.
- [12] M. Farina, A. Di Donato, T. Monti, T. Pietrangelo, T. Da Ros, A. Turco, et al., "Tomographic effects of near-field microwave microscopy in the investigation of muscle cells interacting with multi-walled carbon nanotubes," *Appl. Phys. Lett.*, vol. 101, p. 203101, 2012.
- [13] J. J. Kopanski, L. You, J.-J. Ahn, E. Hitz, and Y. S. Obeng, "Scanning Probe Microscopes for Subsurface Imaging," *ECS Transactions*, vol. 61, pp. 185-193, 2014.